**Supplemental *Appendix,* Table 1.** List of primers for genotyping.

| Alleles/Transgenes | Primer |
|---|---|
| Waved 2 | wave2-F: 5′-ATAACCTGACACTTGTCAGAGTAC-3′<br>wave2-R: 5′-TTTGCAATCTGCACACACCAGTTG-3′ |
| EGFR-flox | EGFR-S: 5′-CTTTGGAGAACCTGCAGATC-3′<br>EGFR-AS: 5′-CTGCTACTGGCTCAAGTTTC-3′ |
| CD11b-Cre | CD11b-CreF: 5'-AATGCTTCTGTCCGTTTGC-3'<br>CD11b-CreR: 5'- CGGCAACACCATTTTTTCTG-3' |
| ACTA1-Cre | oIMR1084: 5'-GCGGTCTGGCAGTAAAAACTATC-3'<br>oIMR1084: 5'- GTGAAACAGCATTGCTGTCACTT-3'<br>oIMR 7338: 5'- CTAGGCCACAGAATTGAAAGATCT-3'<br>oIMR 7339: 5'- GTAGGTGGAAATTCTAGCATCATCC-3' |
| Adipoq-Cre | Adipoq-CreF: 5'-ACGGACAGAAGCATTTTCCA-3'<br>Adipoq-CreR: 5'-GGATGTGCCATGTGAGTCTG-3' |
| Alb1-Cre | Albumin-CreF: 5′-ACCTGAAGATGTTCGCGATTATCT-3'<br>Albumin-CreR: 5′-ACCGTCAGTACGTGAGATATCTT-3' |
| AREG-/- | AR F1M: 5'-CTTTCCAGCTTTCTCCACCTCAAG -3'<br>AR R1M: 5'-ACAGTAACCTCTGTTGCATGCCAC-3'<br>PGK2: 5'-CTGCACGAGACTAGTGAGACGTGC-3' |

***Supplemental Appendix,* Table 2.** List of antibody, source, application and dilution

| Antibody | Catalog Number | Dilution |
|---|---|---|
| Goat anti-EGFR | Sigma, E1281 | IF 1:50 |
| Rabbit anti-Amphiregulin | Abcam, ab234750 | WB 1:1000; IF 1:100 |
| Rabbit anti-Perilipin-1 | Cell signal technology, 9349 | IF 1:100 |
| Rabbit anti-IL-1β | Abcam, ab9722 | IF 1:100 |
| Rabbit anti-Ki67 | Abcam, ab16667 | IF 1:300 |
| Rat anti-F4/80 | Bio-Rad, MCA497R | IF 1:50 |
| Rabbit anti-CD68 | Abcam, ab125212 | IF 1:100 |
| Rabbit anti-CD206 | Proteintech, 18704-1-AP | IF 1:100 |
| Rabbit anti-Arginase 1 | Novus biologicals, NBP1-32731 | IF 1:100 |
| Rabbit anti-p-AKT | Cell signal technology, 4046 | WB 1:1000; IF 1:100 |
| Rabbit anti-AKT | Cell signal technology, 4685 | WB 1:1000 |
| Mouse anti-α-Tubulin | Cell signal technology, 3873 | WB 1:2000 |
| Mouse anti-TNF-a | Santa Cruz, SC-133192 | IF 1:50 |
| Rabbit anti-CX3CR1 | Abcam, ab8021 | IF 1:100 |
| Anti-mouse CD45 (30-F11) | Biolegend 103149 | FC 0.2 mg/ml |
| Anti-mouse/human CD11b (M1/70) | Biolegend 101226 | FC 0.2 mg/ml |
| Anti-mouse F4/80 (BM8) | Biolegend 123130 | FC 0.2 mg/ml |
| Purified anti-mouse CD16/32 (93) | Biolegend 101302 | FC 0.2 mg/ml |
| Anti-mouse CD170 (1RNM44N) | eBioscience, 56170280 | FC 0.2 mg/ml |
| Anti-mouse Ly-6G (1A8) | Biolegend 127614 | FC 0.2 mg/ml |
| Anti-mouse CD9 (MZ3) | Biolegend 124808 | FC 0.2mg/ml |
| Anti-mouse CD64 (X54-5/7.1) | Biolegend 139308 | FC 0.2mg/ml |
| Anti-mouse CD170 (S17007L) | Biolegend 155506 | FC 0.2mg/ml |
| Anti-mouse CD8a (53-6.7) | Biolegend 100708 | FC 0.2mg/ml |
| Anti-mouse CD19 (6D5) | Biolegend 115508 | FC 0.2mg/ml |
| Anti-mouse CD3e (145-2C11) | Biolegend 100308 | FC 0.2mg/ml |
| Anti-mouse Ly6c (HK 1.4) | Biolegend, 128024 | FC 0.2mg/ml |
| Rabbit anti-CD9 | ThermoFisher, MA531980 | IF 1:50 |

***Supplemental Appendix,*** **Table 3.** List of gene probes (Applied Biosystems)

| Mouse primer | Catalog Number |
|---|---|
| *Emr1* | Mm00802529 |
| *Cd68* | Mm03047343 |
| *Tnf* | Mm99999068 |
| *Il1b* | Mm00434228 |
| *Il6* | Mm00446190 |
| *Ccl2* | Mm00441242 |
| *Col1a1* | Mm00801666 |
| *Col3a1* | Mm01254476 |
| *Col4a1* | Mm01210125 |
| *Acta2* | Mm01546133 |
| *Tgfb1* | Mm00441726 |
| *Ctgf* | Mm01192933 |
| *Nos2* | Mm00440502 |
| *Cd206* | Mm01329362 |
| *Arg1* | Mm00475991 |
| *Il4ra* | Mm01275139 |
| *Cd209* | Mm00460067 |
| *Ccl2* | Mm00441242 |
| *Ccl3* | Mm00441258 |
| *Ccr1* | Mm01216147 |
| *Ccr2* | Mm01216173 |
| *Ccr5* | Mm04207879 |
| *Cx3cl1* | Mm00436454 |
| *Cxcl12* | Mm00445553 |
| *Cxcl1* | Mm04207460 |
| *Cxcl2* | Mm00436450 |
| *Cx3cr1* | Mm00438354 |
| *Cxcr4* | Mm01292123 |
| *Egfr* | Mm00433023 |
| *Erbb2* | Mm00658541 |
| *Erbb3* | Mm01159999 |
| *Erbb4* | Mm01256793 |
| *Egf* | Mm01316968 |
| *Tgf a* | Mm00446232 |
| *Hb-egf* | Mm00439307 |
| *Areg* | Mm00437583 |
| *Btc* | Mm00432137 |
| *Ereg* | Mm00514794 |
| *Epgn* | Mm00504344 |
| *Lep* | Mm00434759 |
| *Adipoq* | Mm00456425 |
| *Hif1a* | Mm00468869 |
| *Pgk1* | Mm00435617 |
| *Ldha* | Mm01612132 |

| | |
|---|---|
| *Glut1* | Mm00441477 |
| *Hk1* | Mm00439344 |
| *Pkm* | Mm00834102 |
| *Pfdb3* | Mm00504650 |
| *Ucp1* | Mm01244861 |
| *Acta2* | Mm01546133 |
| *Irf5* | Mm00496477 |
| *Il23a* | Mm00518984 |
| *Ym1* | Mm00657889 |
| *Fizz1* | Mm00445109 |

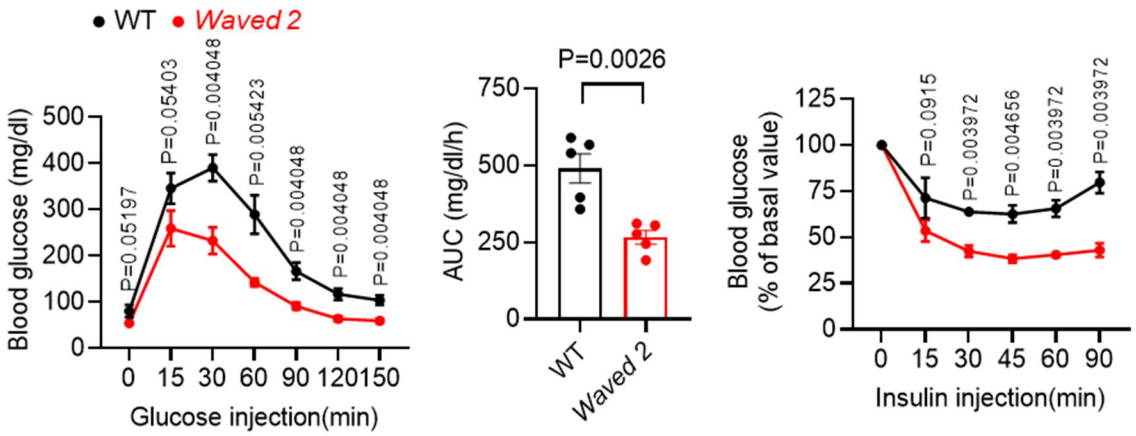


**Supplementary Figure 1. Female *Waved* 2 mice developed less insulin resistance in diet-induced obesity.** Female *Waved* 2 mice with intrinsic EGFR tyrosine kinase deficiency and WT mice were fed the HFD for 12 weeks. Female *Waved 2* mice had improved glucose tolerance test (GTT, n=5) and insulin tolerance test (ITT, n=3).

Data are means ± SEM, analyzed using 2 tailed Student's t test and 2-way ANOVA followed by Tukey's post hoc test for GTT and 2-way ANOVA followed by Tukey's post hoc test for ITT.

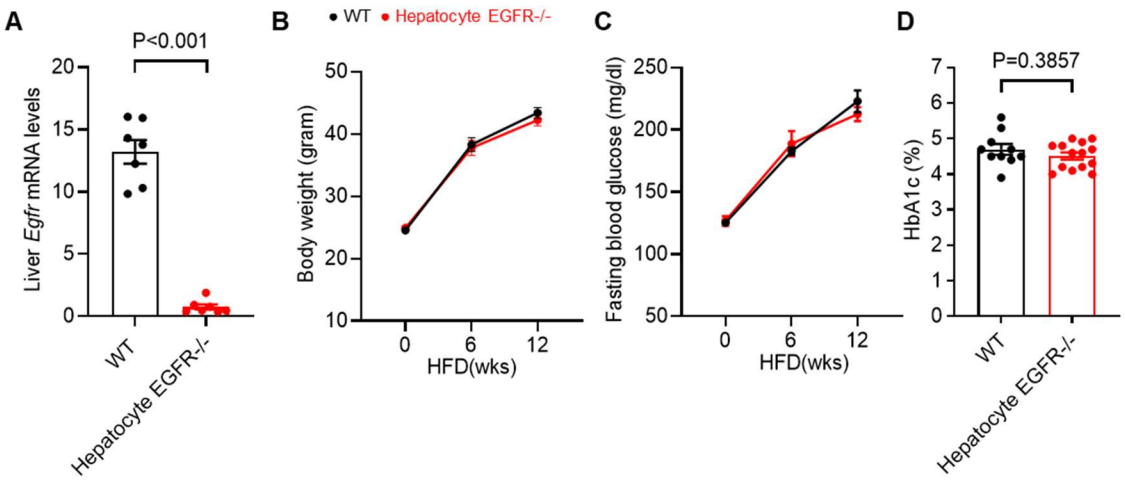


**Supplementary Figure 2. Selective EGFR deletion in hepatocytes had on effect on insulin resistance in diet-induced obesity.** Male hepatocyte EGFR-/- (Alb1-Cre; $EGFR^{f/f}$) mice and WT ($EGFR^{f/f}$) mice were fed with the HFD for 12 weeks. (**A**) Hepatocyte EGFR-/- mice had markedly lower liver *Egfr* mRNA levels compared to WT mice. N=7. (**B** and **C**) Hepatocyte EGFR-/- mice and WT mice had similar body weight gain (**B**) and fasting blood glucose (**C**) after the HFD treatment. N=10 and 14. (**D**) Hepatocyte EGFR-/- mice and WT mice had similar HbA1c at 12 weeks after the HFD. N= 10 and 14.

Data are means ± SEM, analyzed using 2 tailed Student's t test for **A** and **D**; 2-way ANOVA followed by Tukey's post hoc test for **B** and **C**.

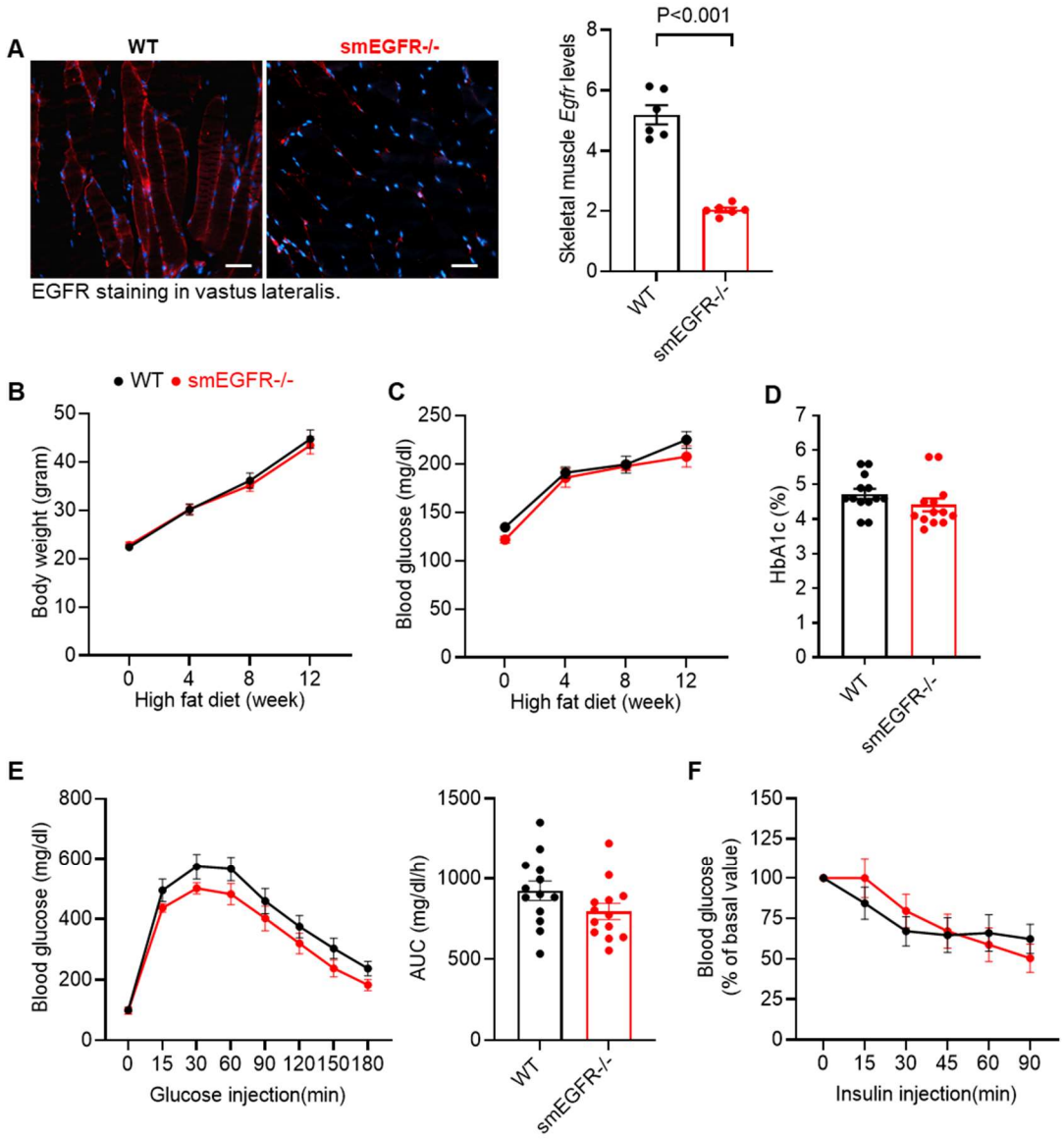


**Supplementary Figure 3. Selective deletion of EGFR in skeletal muscle had on effect on insulin resistance in diet induced obesity.** Male smEGFR-/- (ACTA1-Cre; $EGFR^{f/f}$) mice and WT ($EGFR^{f/f}$) mice were fed with the HFD for 12 weeks. (**A**) Both EGFR mRNA and protein levels in vastus lateralis were decreased in smEGFR-/- mice compared to WT mice. N=6. Scale bar=100μm. (**B-D**) smEGFR-/- mice and WT mice had similar body weight gain (**B**), fasting blood glucose (**C**), and HbA1c (**D**). N=13. (**E** and **F**) smEGFR-/- mice and WT mice had similar glucose tolerance test (GTT, n=13) (**E**) and insulin tolerance test (ITT, n=7) (**F**).

Data are means ± SEM, analyzed using 2 tailed Student's t test for **A and D**, 2-way ANOVA followed by Tukey's post hoc test for **B, C**, and **F;** and 2 tailed Student's t test and 2-way ANOVA followed by Tukey's post hoc test for **E**.

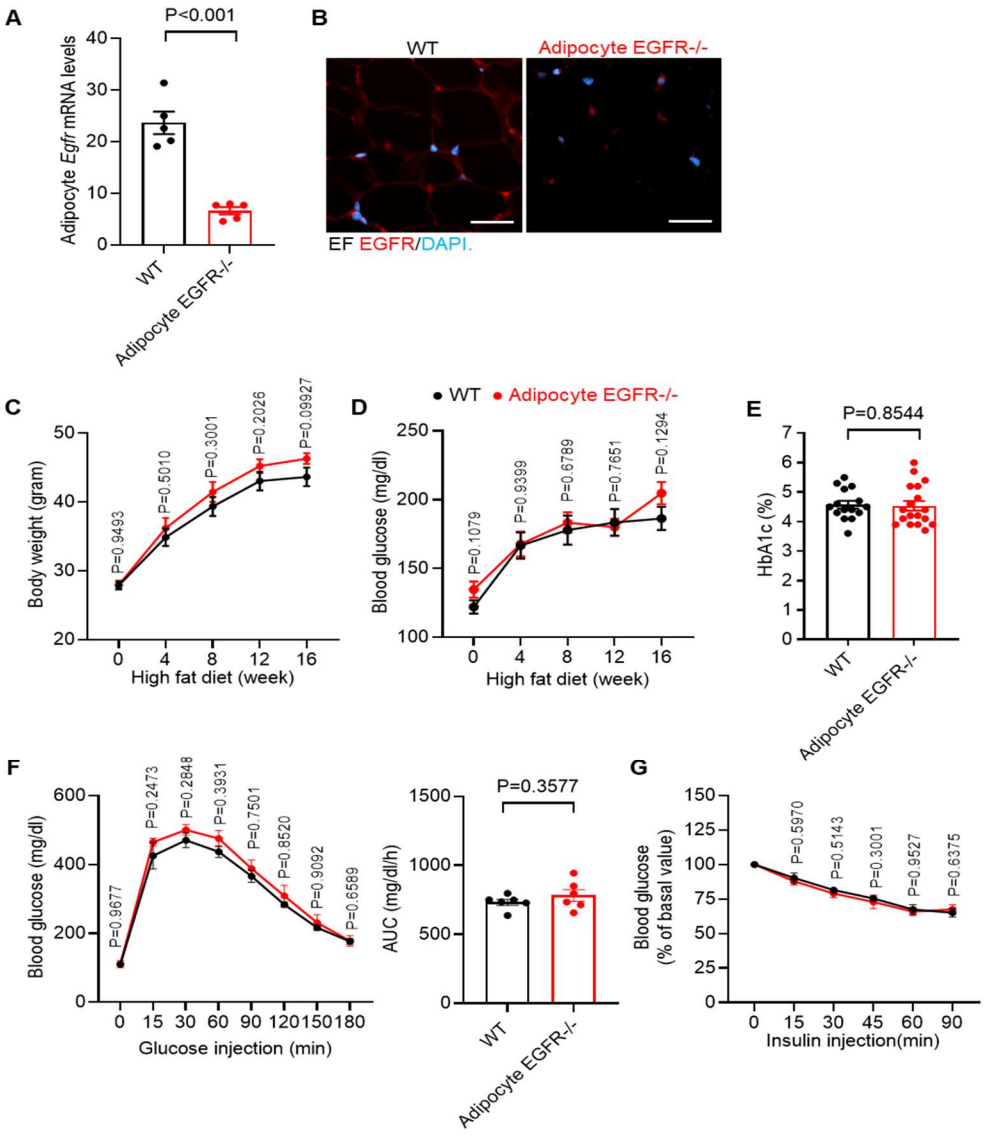


**Supplementary Figure 4. Selective deletion of EGFR in adipocytes in male mice had on effect on insulin resistance in diet induced obesity.** Male Adipocyte EGFR-/- (Adipoq-Cre; $EGFR^{f/f}$) mice and WT ($EGFR^{f/f}$) mice were fed with the HFD for 16 weeks. (**A and B**) EF EGFR mRNA (**A**) and protein (**B**) expression was markedly decreased in adipocyte EGFR-/- mice compared to WT mice. N=5. Scale bar=100μm. (**C-E**) Adipocyte EGFR-/- mice and WT mice had similar body weight gain (n=15) (**C**), fasting blood glucose (n=15) (**D**), and HbA1c (N=15 and 17) (**E**). (**F and G**) Adipocyte EGFR-/- mice and WT mice had similar glucose tolerance test (n=6 and 8) (**F**) and insulin tolerance test (n=6) (**G**).

Data are means ± SEM, analyzed using 2 tailed Student's t test for **A** and **E;** 2-way ANOVA followed by Tukey's post hoc test for **C**, **D**, and **G;** and 2 tailed Student's t test and 2-way ANOVA followed by Tukey's post hoc test for **F**.

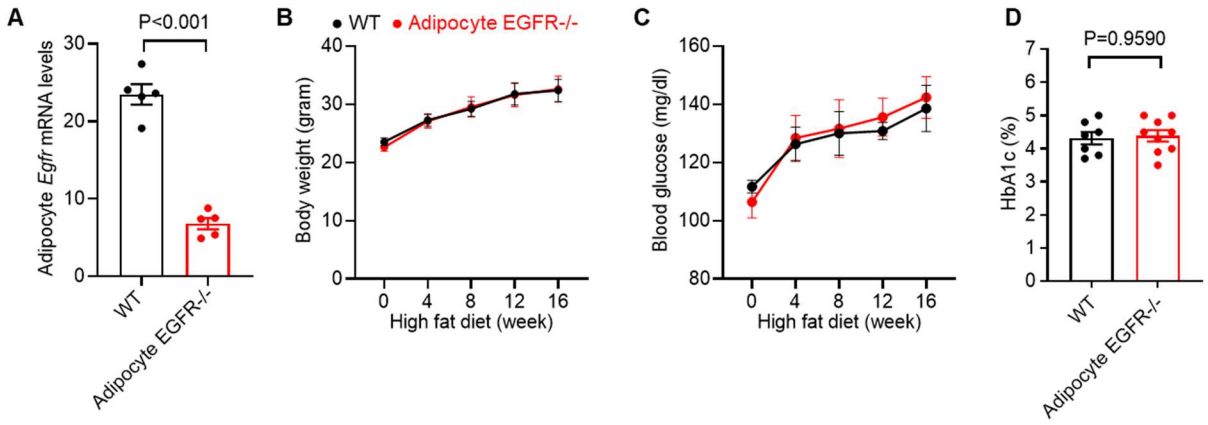


**Supplementary Figure 5. Selective deletion of EGFR in adipocytes in female mice had no effect on insulin resistance in diet induced obesity.** Female Adipocyte EGFR-/- (Adipoq-Cre; $EGFR^{f/f}$) mice and WT ($EGFR^{f/f}$) mice were fed with the HFD for 16 weeks. (**A**) Inguinal EGFR mRNA expression was markedly decreased in adipocyte EGFR-/- mice compared to WT mice. N=5. (**B**-**D**) Female adipocyte EGFR-/- mice and WT mice had similar body weight gain (**B**), fasting blood glucose (**C**), and HbA1c (**D**). N=7 and 9.

Data are means ± SEM, analyzed using 2 tailed Student's t test for **A** and **D,** 2-way ANOVA followed by Tukey's post hoc test for **B and C.**

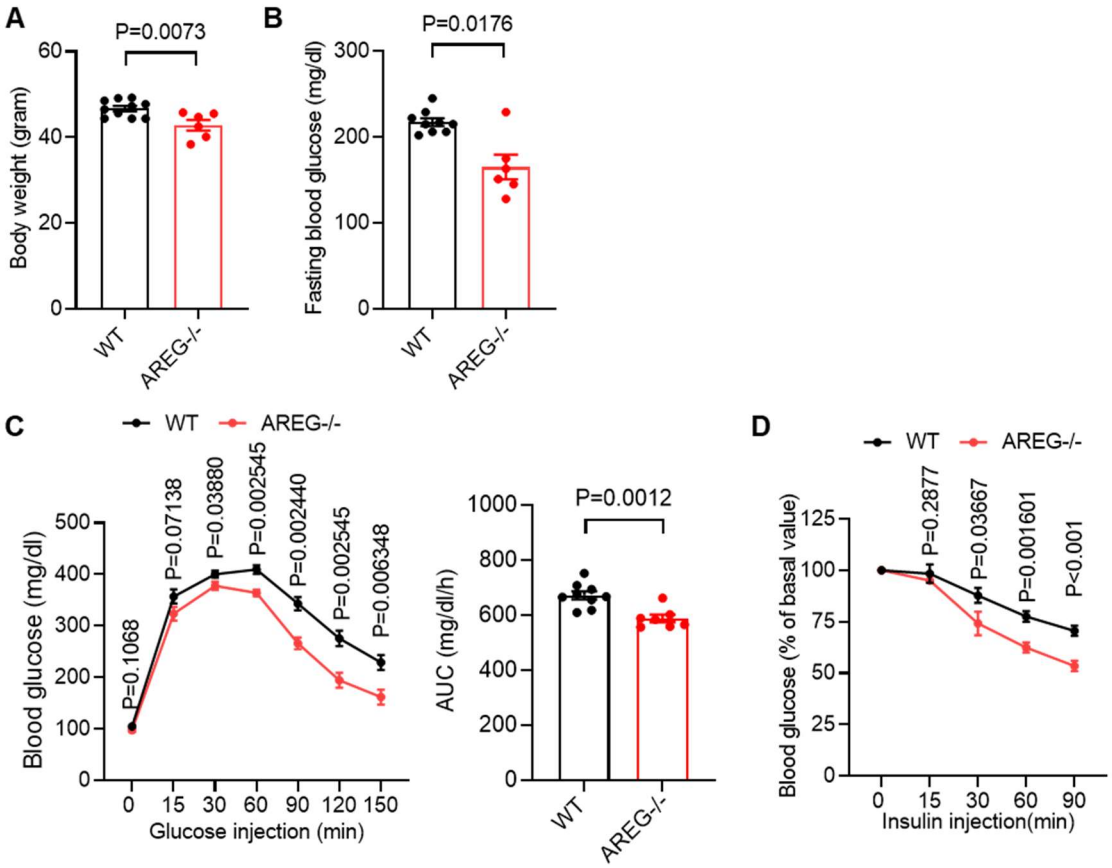


**Supplementary Figure 6. AREG deletion protected against insulin resistance in response to a high fat diet**. WT and global AREG-/- mice were fed with the HFD for 12 weeks. (**A** and **B**) Global AREG-/- mice had lower body weight (**A**) and lower fasting blood glucose (**B**). N=6 and 10. (**C** and **D**) Global AREG-/- mice had improved glucose tolerance (n=7 and 9) (**C**) and insulin tolerance (n=6 and 9) (**D**).

Data are means ± SEM, analyzed using 2 tailed Student's t test for **A and B**; 2 tailed Student's t test and 2-way ANOVA followed by Tukey's post hoc test for **C;** and 2-way ANOVA followed by Tukey's post hoc test for **D.**

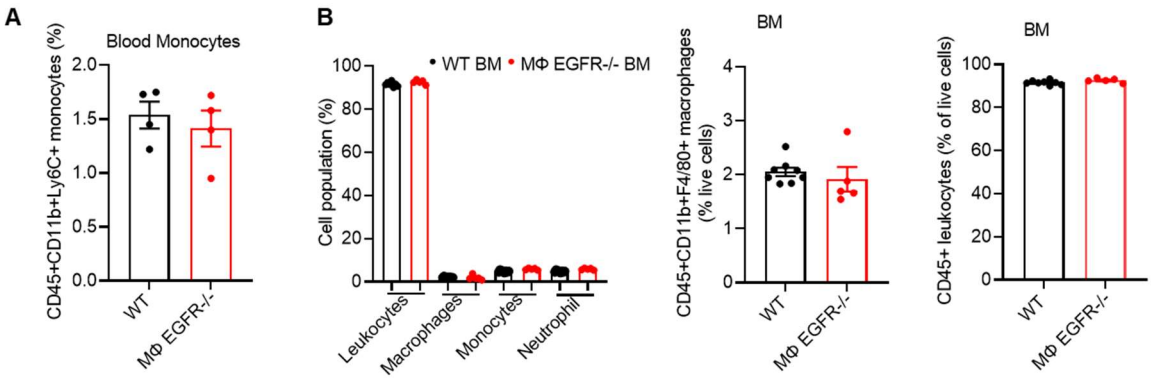


**Supplementary Figure 7**. Myeloid EGFR deletion had no effect on blood monocyte counts and bone marrow leukocyte composition. Control WT and MΦ EGFR-/- mice were used. (**A)** Flow cytometry determined no differences in the monocyte (CD45+; CD11b+; Ly6C+) population from peripheral blood isolated from WT and MΦ EGFR-/- mice. N=4. (**B)** Flow cytometry also confirmed no significant changes in leukocyte (CD45+), macrophage (CD45+; CD11b+; F4/80+), monocyte (CD45+; CD11b+; F4/80dim; Ly6C+), and neutrophil (CD45+; CD11b+; Ly6G+) bone marrow cell populations relative to total alive bone marrows cells. N=5 and 8.

Data are means ± SEM, analyzed using 2 tailed Student's t test.

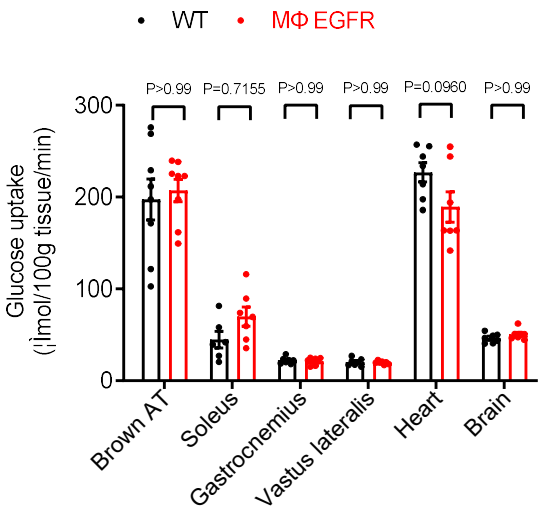


**Supplementary Figure 8. Myeloid EGFR deletion had no effect on glucose uptake in any tissues except for white adipose tissues in diet-induced obesity.** WT and myeloid EGFR-/- mice were on the HFD for 12 weeks, and hyperinsulinemic-euglycemic clamps were performed. Glucose uptake, a marker of insulin resistance, was comparable in brown AT, skeletal muscles (soleus, gastrocnemius, and vastus lateralis), and heart and brain.

Data are means ± SEM, n=7 and 8, analyzed using 2 tailed Student's t test.

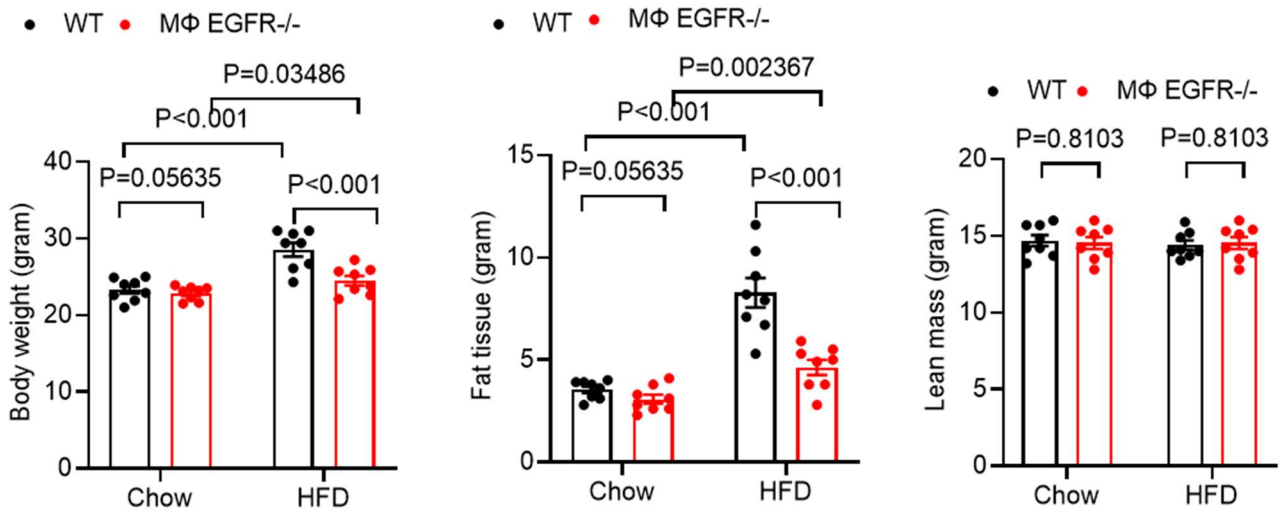


**Supplementary Figure 9.** High fat diet led to reduced fat mass increases in myeloid EGFR-/- mice. Body composition was determined by NMR in MΦ EGFR-/- mice and littermate WT mice with chow food and with HFD for 4 weeks. Body weight, fat tissue mass and lean mass were comparable between WT and MΦ EGFR-/- mice with chow food diet. HFD for 4 weeks led to less increased body weight and fat tissue mass in MΦ EGFR-/- mice compared to WT mice. N=8.

Data are means ± SEM, analyzed using 2-way ANOVA followed by Bonferroni's post hoc test.

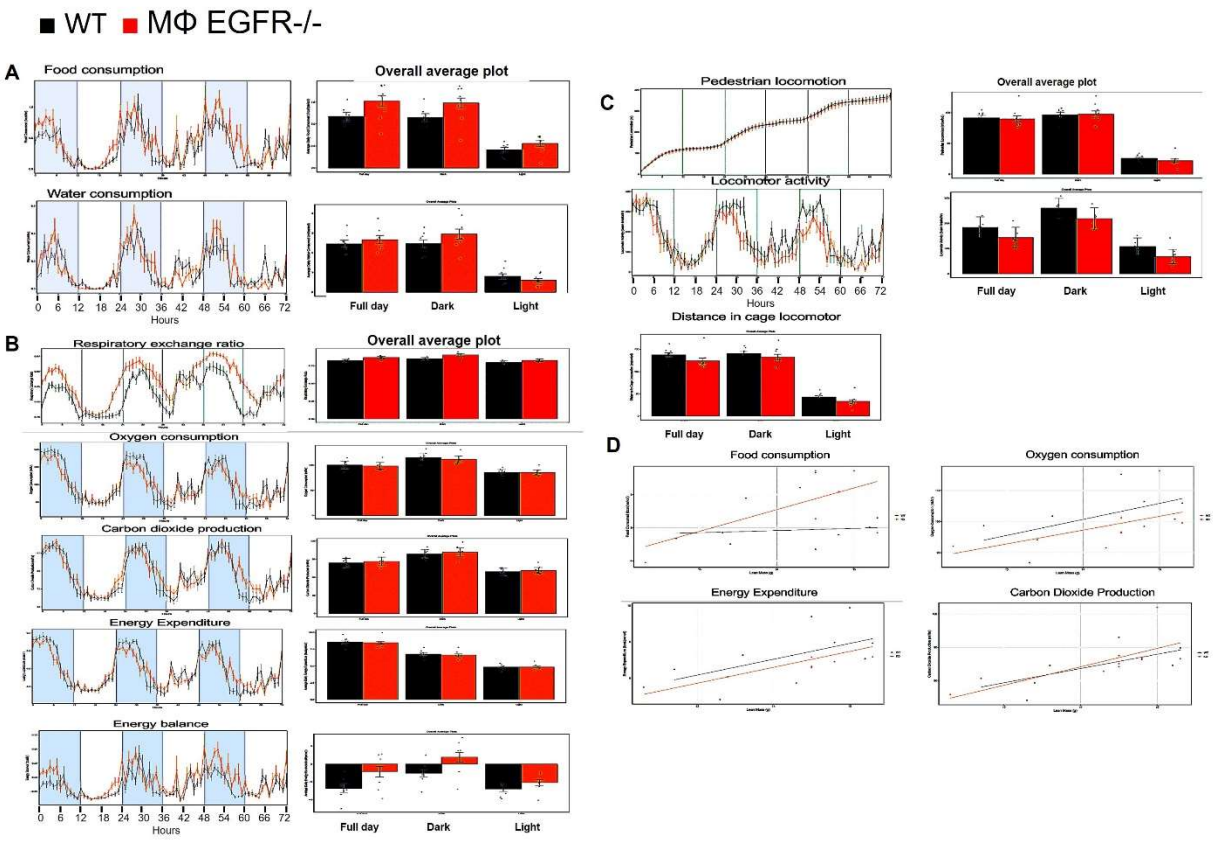


**Supplementary Figure 10.** WT and myeloid EGFR-/- mice had similar metabolic parameters on chow food diet. We assessed energy balance by indirect calorimetry experiment with Promethion Systems in WT and MΦ EGFR-/- mice fed chow food. (**A**-**C)** No differences were observed in food ingestion and circadian rhythm of feeding (**A**), respiratory exchange ratio, oxygen consumption, carbon dioxide production, energy expenditure, energy balance (**B**), ambulatory/pedestrian locomotion, locomotor activity, and distance in cage locomotor between WT mice and MΦ EGFR-/- mice (**C**). Shaded areas indicate the dark photoperiod. Data are presented by mean ± SEM; n=not significant, by 2-way ANOVA followed by Bonferroni's post hoc test, n=8 in each group. **(D)** Regression plot of food consumption, oxygen consumption, energy expenditure, and carbon dioxide production vs. lean mass. N=8, ANCOVA was used.

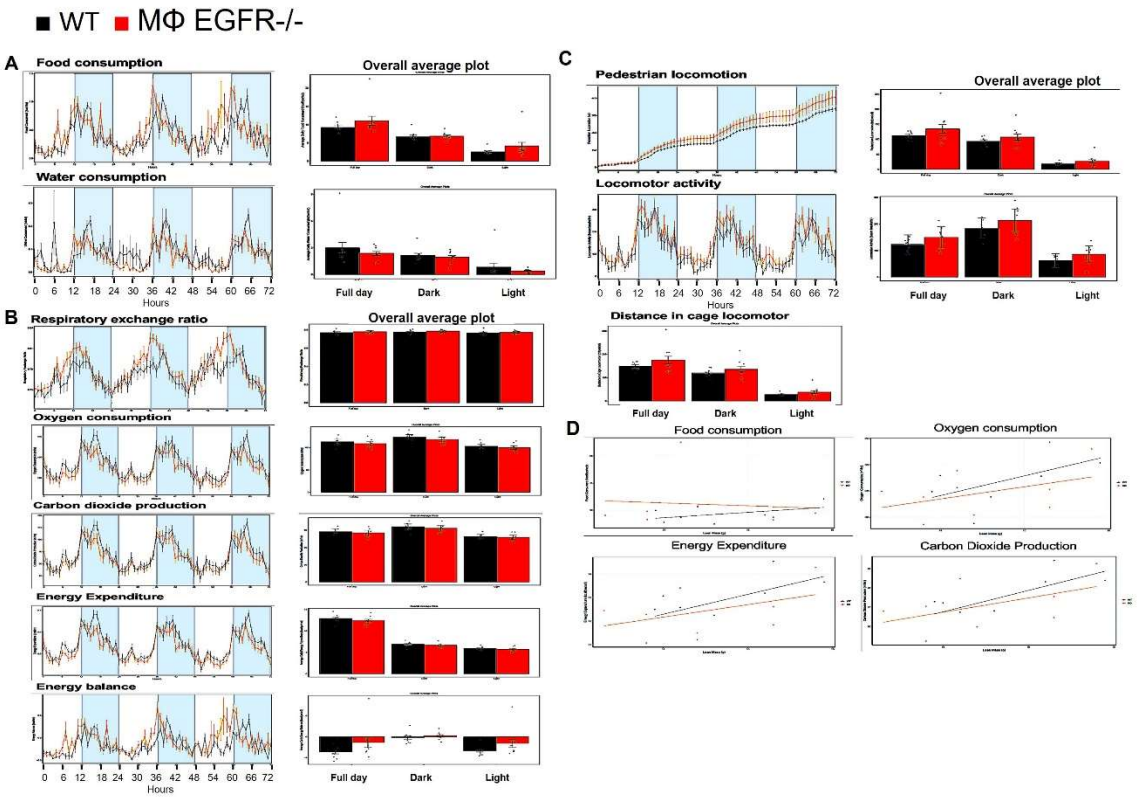


**Supplementary Figure 11.** WT and myeloid EGFR-/- mice had similar metabolic parameters after 4 weeks on the high fat diet. We assessed energy balance by indirect calorimetry experiment with Promethion Systems in WT and MΦ EGFR-/- mice fed HFD for 4 weeks. (**A**-**C)** No differences were observed in food ingestion and circadian rhythm (**A**), respiratory exchange ratio, oxygen consumption, carbon dioxide production, energy expenditure or energy balance (**B**) between WT mice and MΦ EGFR-/- mice although there was trend for increased ambulatory/pedestrian locomotion, locomotor activity, and distance in cage locomotor in the MΦ EGFR-/- mice (**C**). Shaded areas indicate the dark photoperiod. Data are presented by mean ± SEM; by 2-way ANOVA followed by Bonferroni's post hoc test, n=8 in each group. (**D**) Regression plot of food consumption, oxygen consumption, energy expenditure, and carbon dioxide production vs. lean mass. N=8, ANCOVA was used.

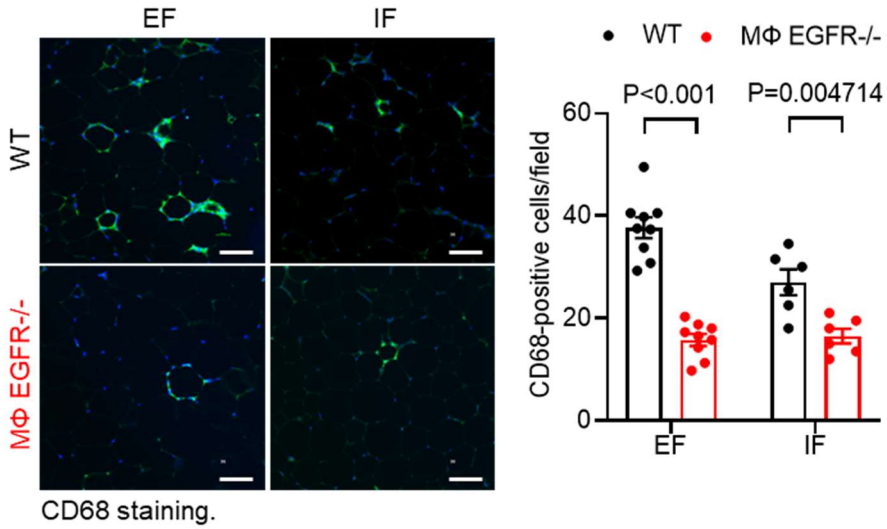


**Supplementary Figure 12. Mice with myeloid EGFR deletion had fewer ATMs in diet-induced obesity.** Male WT and myeloid EGFR-/- mice were fed the HFD for 12 weeks. CD68 immunofluorescent staining showed that myeloid EGFR-/- mice had decreased ATMs in both EF and IF. N=6. Scale bar=100μm.

Data are means ± SEM, analyzed using 2-way ANOVA followed by Bonferroni's post hoc test.

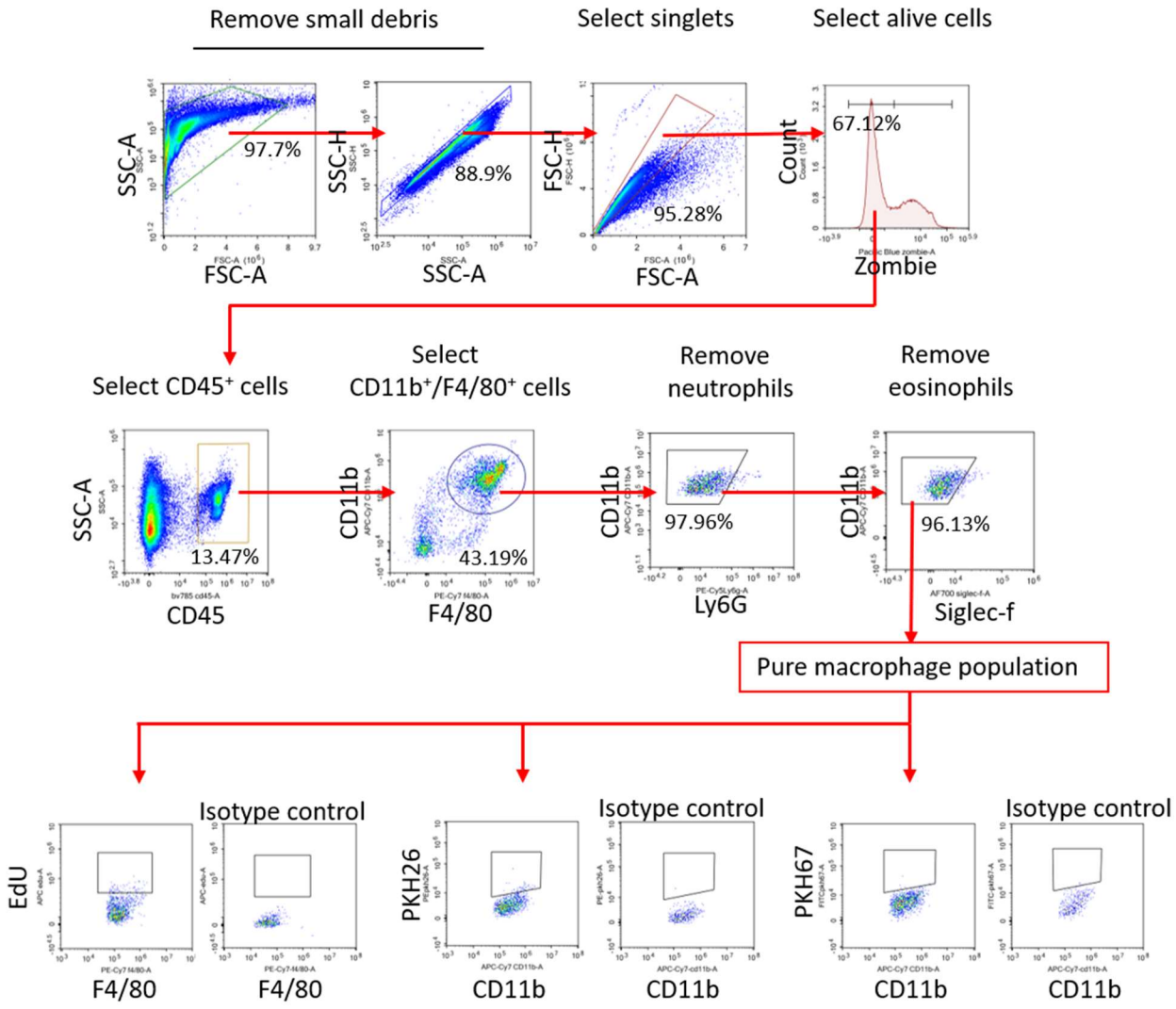


**Supplementary Figure 13. Gating strategy of Figure 7B for epididymal fat tissue ATM population, monocyte recruitment, and ATM proliferation analysis.**

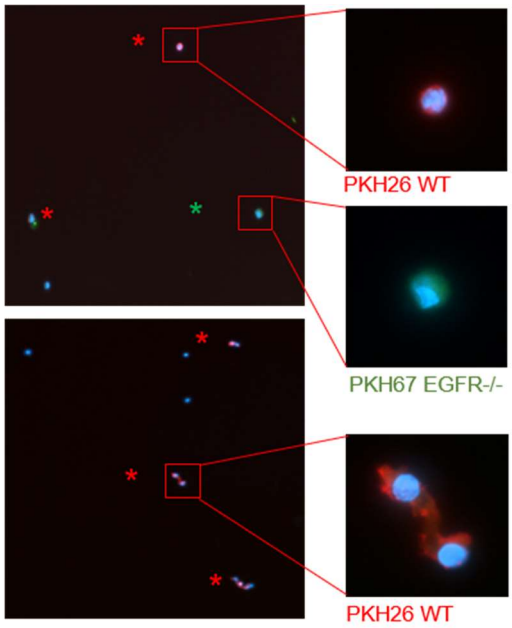


**Supplementary Figure 14. Bone marrow derived monocyte (BMDMs) with EGFR deletion had impaired recruitment in WT mice in diet-induced obesity.** WT BMDMs were labeled with the monocyte tracking dye PKH26 (red) and EGFR-/- BMDMs with PKH67 (green) and injected a mixture containing equal amounts of labeled WT and EGFR-/- BMDMs into WT recipients fed the HFD for 6 weeks. More PKH26-positive WT BMDMs were also observed in cell suspension smears of EF from WT recipients (representative of 3 independent experiments).

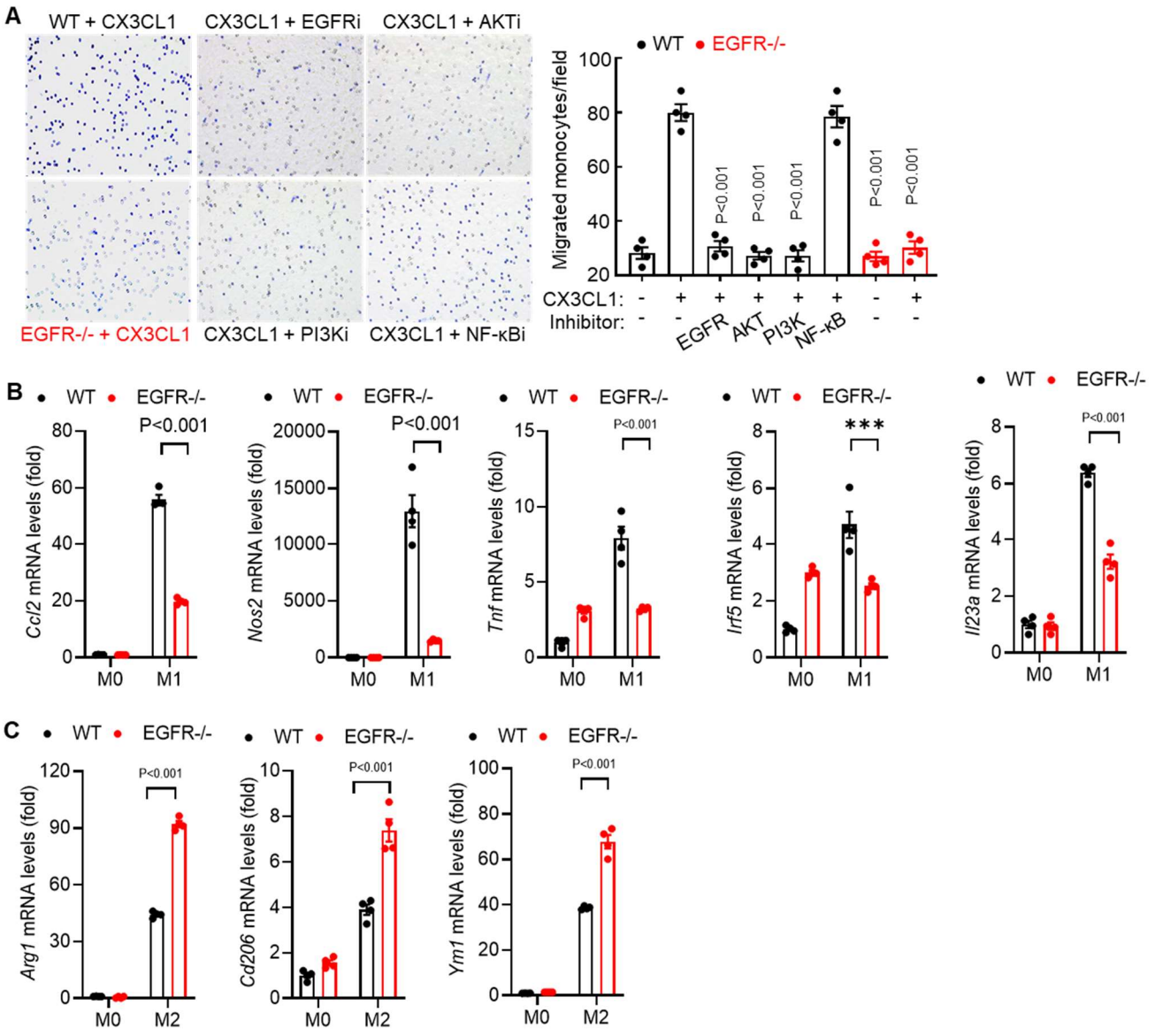


**Supplementary Figure 15. EGFR signaling regulated BMDM migration and polarization.** BMDMs were isolated from WT and MΦ EGFR-/- mice. (**A**) Chemoattractant CX3CR1-induced migration in WT BMDMs was blocked by an EGFR inhibitor (erlotinib), an AKT inhibitor (MK-2206), a PI3K inhibitor (BEZ235) or EGFR deletion. N=4. (**B** and **C**) EGFR-/- BMDMs had lower proinflammatory M1/Th1 cytokines/chemokines with LPS/IFN-γ-mediated M1 polarization, including *Ccl2*, *Nos2*, *Tnf*, and *Il23a* (**B**) but higher anti-inflammatory cytokines with IL-4/IL-13-mediated M2 polarization, including *Arg1*, *Cd206*, and *Ym1* (**C**). N = 4 in each group.

Data are means ± SEM, analyzed using 2-way ANOVA followed by Bonferroni's post hoc test for all.

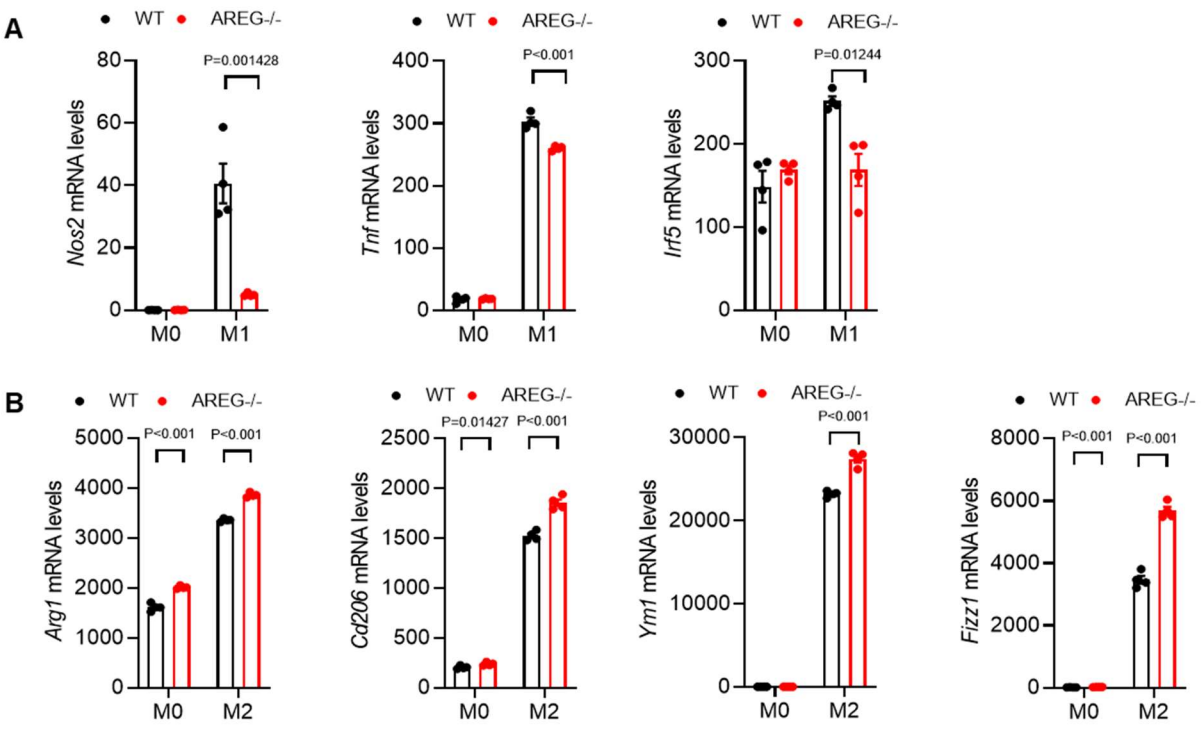


**Supplementary Figure 16. AREG regulated BMDM polarization.** BMDMs were isolated from WT and global AREG-/- mice. (**A** and **B**) AREG-/- BMDMs had lower proinflammatory M1/Th1 cytokines/chemokines with LPS/IFN-γ-mediated M1 polarization, including *Nos2*, *Tnf*, and *Irf5* (**A**) but higher anti-inflammatory cytokines with IL-4/IL-13-mediated M2 polarization, including *Arg1*, *Cd206*, *Fizz1*, and *Ym1* (**D**). N = 4 in each group.

Data are means ± SEM, analyzed using 2-way ANOVA followed by Bonferroni's post hoc test for all.

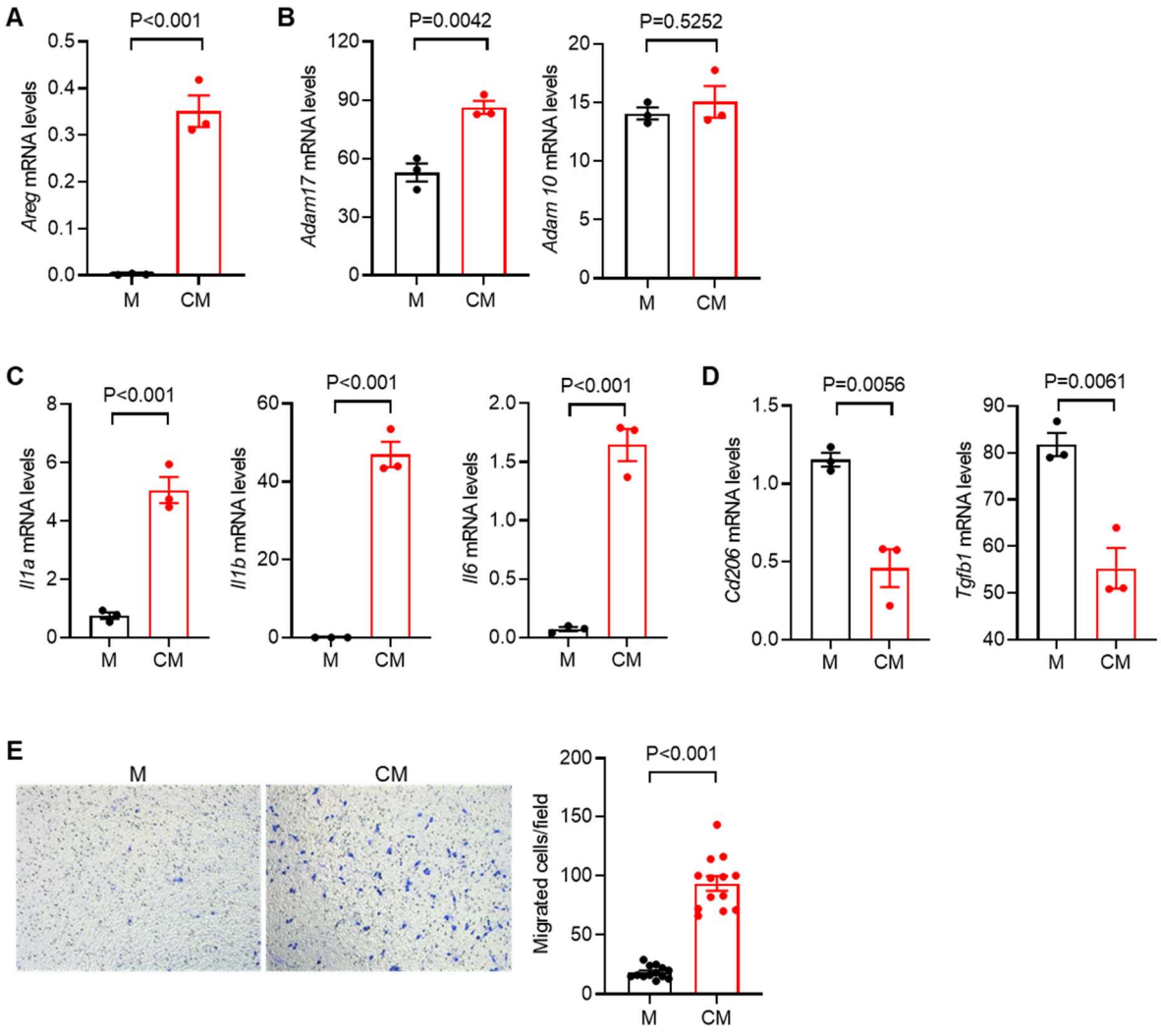


**Supplementary Figure 17. Adipocytes regulated macrophage properties.** Apoptotic 3T3-L1 cell differentiated adipocytes and mouse macrophage-like RAW264.7 cells were used. **(A-D)** Compared to serum-free medium (M), conditional serum-free medium (CM) from apoptotic adipocytes stimulated RAW264.7 cell mRNA expression of *Areg* (**A**), *Adam17* (**B**), proinflammatory cytokines including *Il1a*, *Il1b*, and *Il6* (**C**), and inhibited antiinflammatory *Cd206* and *Tgfb* (**D**). N=3. (**E**) Coculture with apoptotic adipocytes led to increased RAW264.7 cell migration. N=13.

Data are means ± SEM, analyzed using 2 tailed Student's t test.

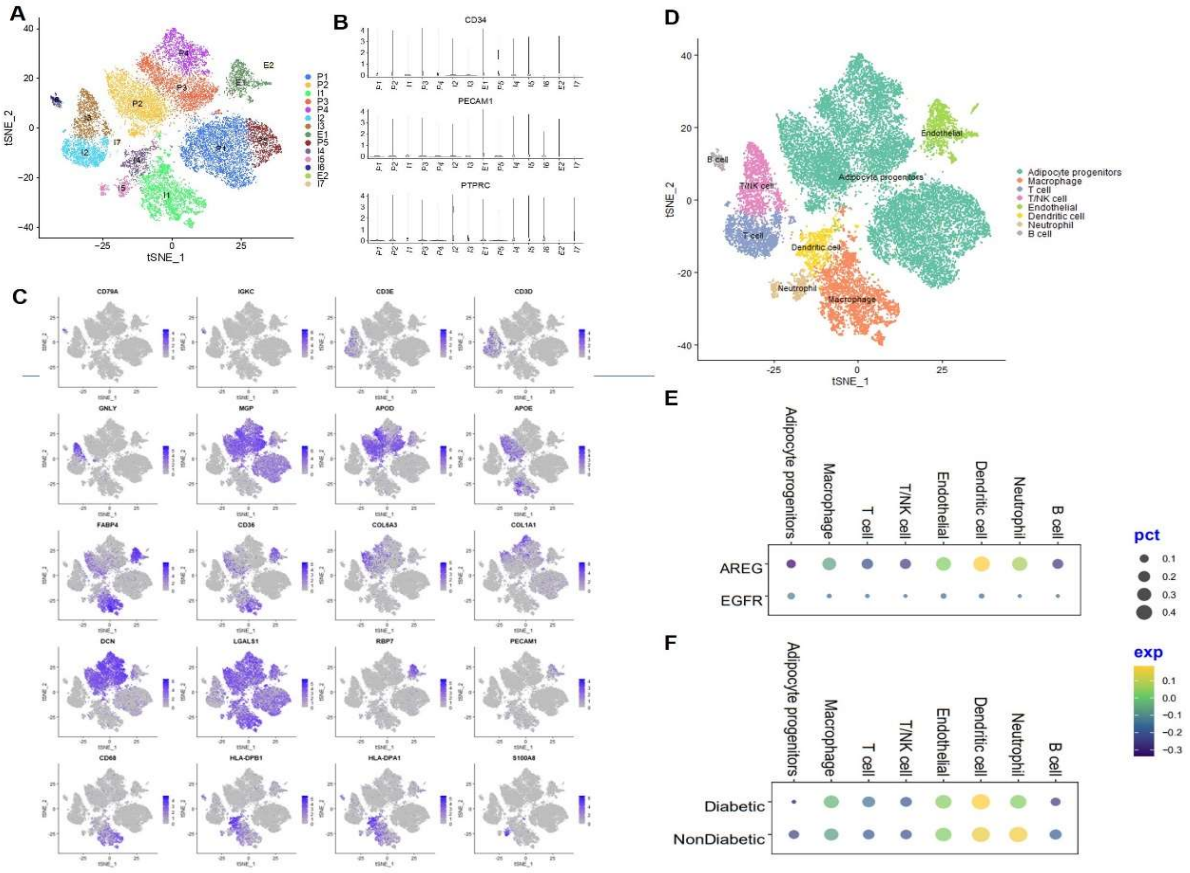


**Supplementary Figure 18**. *AREG* mRNA levels were increased in human adipose tissue macrophages and dendritic cells in individuals with type 2 diabetes. **A**. Identified cell populations in the non-adipocyte fraction of adipose tissue from database (GSE129363)[27]. Fourteen clusters were identified from 26,350 cells derived from SVF (stromal vascular fraction) of 25 adipose samples, including progenitors (P1–P5), immune cells (I1–I7) and endothelial cells (E1–E2). **B**. SVF-derived progenitor clusters. Violin plots of log-transformed expression density of *CD34*, *CD31/PECAM1* and *CD45/PTPRC* across all SVF clusters from 25 samples. The width of the violin plot indicates the number of cells expressing the particular gene. **C**. Cell type annotation indicated cell populations classified as immune cells. **D**. Six clusters of immune cells were identified, macrophages, T cells, T/NK cells, dendritic cells, neutrophils, and B cells. **E**. *AREG* transcripts were evident in macrophages, dendritic cells, neutrophils, and endothelial cells. **F**. Macrophage and dendritic cell *AREG* transcripts were higher in diabetic adipose tissue than in non-diabetic adipose tissue.

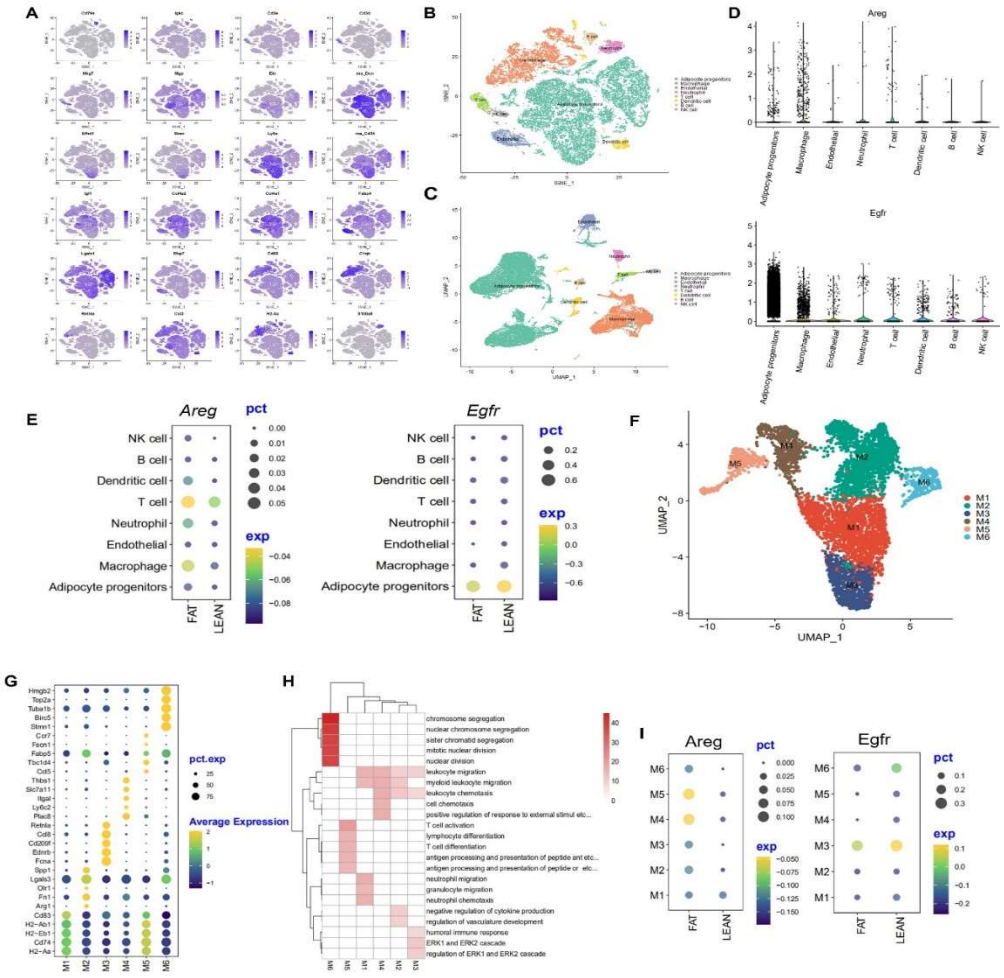


**Supplementary Figure 19.** *Areg* mRNA levels were increased in adipose tissue macrophages in high fat diet induced obese mice. **A**. Cell type annotation for cell populations from epididymal fat tissue stromal vascular fraction (SVF) of lean and fat mice from GSE16187 database[28]. **B**. Clustering results indicated six clusters of immune cell populations including macrophages, T cells, NK cells, dendritic cells, neutrophils, and B cells. **C**. Uniform manifold approximation and projection (**UMAP**) plot for unsupervised clustering of the single cells identified a total of 8 cell populations. **D**. Both *Areg* and *Egfr* transcripts were mainly expressed in adipocyte progenitors and macrophages. **E**. *Areg* transcripts were increased in macrophages, dendritic cells, neutrophils, and T cells in SVF from obese mice. There were no differences in *Egfr transcripts* between lean and obese mice. **F**. UMAP plot for unsupervised clustering of the single cells identified a total of 6 macrophage populations (M1-M6). G. Bubble map shows the top genes in all macrophage subgroups. **H**. Gene ontology analysis of the M1 to M6 macrophage subgroups. **I**. *Areg* transcripts were most increased in M4 and M5 subgroups in obese mice. GO analysis revealed M4 and M5 subgroups are involved in leukocyte migration and T cell activation. There were no differences in *Egfr* transcripts in macrophage subgroups between lean mice and obese mice.